



Electrospun nanofibers with a core-shell structure of silicon nanoparticles and carbon nanotubes in carbon for use in lithium-ion battery anodes

Journal:	<i>Journal of Materials Chemistry A</i>
Manuscript ID:	TA-ART-05-2014-002348.R1
Article Type:	Paper
Date Submitted by the Author:	14-Jul-2014
Complete List of Authors:	Nguyen, Hieu; Hankyung National University, Chemical engineering; Korea Research Institute of Chemical Technology, Advanced Materials Division Suk, Jungdon; Korea Research Institute of Chemical Technology, Advanced Materials Division Kim, Dong Wook; Korea Research Institute of Chemical Technology, Advanced Materials Division Park, jun seo; Hankyung National University, Chemical engineering Kang, Yongku; Korea Research Institute of Chemical Technology, Advanced Materials Division

Electrospun nanofibers with a core-shell structure of silicon nanoparticles and carbon nanotubes in carbon for use in lithium-ion battery anodes†

Nguyen Trung Hieu,^{a,b} Jungdon Suk,^b Dong Wook Kim,^b Jun Seo Park^{*a} and Yongku Kang,^{**b}

Abstract

Core-shell structured nanofibers, consisting of silicon nanoparticles and carbon nanotubes encased in carbon (SCNFs), were fabricated for use as an anode material in lithium-ion batteries (LIBs). This entailed first electrospinning precursor solutions containing a blend of silicon nanoparticles (SiNPs), carbon nanotubes (CNTs), and polyvinylpyrrolidone (PVP) for the core; and polyacrylonitrile (PAN) for the shell. The final SCNF structure was obtained by carbonization at 1000 °C for 1 h under nitrogen; the core-shell structure achieved with varying carbon contents being determined by scanning electron microscopy, transmission electron microscopy, and water contact angle measurements. An evaluation of the electrochemical performance of SCNF-based anodes in LIBs found that a SCNF electrode with 1 wt% CNTs has an initial delithiation capacity as high as 1500 mAh/g at C/10 rate, and a retained capability of 50 % at high rate (10C). Following the 100th cycle at 1C, a capacity of 1000 mAh/g and coulombic efficiency of 99 % were achieved, the former representing 74.1 % of the original capacity (1350 mAh/g). Thus, not only does the robust carbon shell of SCNFs minimize the effect of volume expansion in the SiNPs; but the CNTs in the core also provide a greater number of conductive pathways, both between SiNPs and to the carbon shell, which assist electrochemical reactions.

Introduction

High-energy lithium ion batteries (LIBs) have been critical to the development of consumer electronics, electric vehicles, mobile electronic devices, and grid-scale stationary energy storage.^{1,2} As such, there has been growing demand for further advancements in LIBs with regards to achieving a higher energy density, high power performance, longer cycle life, and greater safety.³⁻⁵ For efficient practical application, the energy density (per weight and volume) and cycle life are the most important factors in reducing the relative cost of LIBs per unit of stored energy;^{2,3} and these not surprisingly have been the major focus of recent battery research. Currently, graphite is the most widely used anode material in commercial LIBs, as it offers the benefits of low cost and long cycle life.⁵ However, its low theoretical specific capacity of 372 mAh/g presents a major obstacle to the varied and extensive research toward advanced LIBs, particularly with regards to anode materials.⁵⁻⁷ In an effort to increase the energy density, silicon (Si) has become widely regarded as an alternative advanced anode material for LIBs, because its theoretical capacity of 4200 mAh/g is the highest known. Although this value is about 10 times greater than that of the commercial graphitic anodes, most Si electrodes suffer from a limited cycle life that is typically in the order of less than a few hundred cycles. This limitation is caused by a severe pulverization that is triggered by a more than 300 % volume change (expansion and shrinkage) during lithium insertion and extraction.^{2-4,8-10} This pulverization of Si is directly associated with a decay in capacity, as repeated volume changes can lead to cracking of the anode, which in turn causes a loss of contact with current collectors and carbon conductors.^{2-4,11-13} This volume change also produces solid electrolyte interphase (SEI) layers on the Si surface, thereby making it mechanically unstable.^{2,3} Moreover, the poor cyclability induced inevitably leads to serious capacity fade during charge/discharge cycling,

especially at high current densities.⁸ Thus, in order to meet the aforementioned requirements of LIBs, it is essential to significantly improve the cycle life of Si by reducing its pulverization, volume change, and the poor electrical connectivity in its matrix.

The issue of pulverization can be overcome through the use of nanostructured Si, as the small size allows for relaxation of the stress generated during volume expansion.³ In taking advantage of this effect, numerous studies have demonstrated an enhanced cycle life through the use of Si nanostructures. This has included such examples as nanowires,¹⁴⁻¹⁹ nanotubes,^{20,21} nanoparticles,²²⁻²⁵ and three-dimensional (3D) porous structures.²⁶⁻²⁸ With regards to volume change, a hollow Si nanostructure can provide an empty interior space for expansion, offering numerous advantages, such as a reduction in diffusion-induced stress, as has been demonstrated in previous studies.²⁹⁻³³ The success in this area has led to the chemical vapor deposition (CVD) technique being developed for the coating of disordered carbon onto the surface of Si nanocomposites, thereby preventing the detachment of Si.^{11,13}

More recently, electrospinning processes have emerged as a viable option for a variety of energy-related applications and devices; offering the ability to produce large quantities of one-dimensional (1D) nanostructures, with fine control over their diameter and composition.^{2,34,35} This has been adapted by a number of researchers to the development of 1D silicon nanofiber structures for advanced anode materials.^{6,8-10,36-39} Furthermore, coaxial electrospinning has been frequently employed to fabricate 1D core-shell structured Si-carbon nanofibers.^{3,4,12,40} In such fibers, a core consisting of Si nanoparticles (SiNPs) is encapsulated by a carbon shell, which can resolve both the pulverization and volume expansion issues of Si anodes.^{3,4} However, inherent low electrical conductivity of Si tends to degrade overall battery performance due to high impedance of electron flow during electrochemical process.⁴¹ An idea of application of CNTs in

silicon-based anode materials has been attractive to minimize the volume change and to increase the electrical conductivity, owing to its advantageous effects such as excellent electrical conductivity and mechanical flexibility.⁴¹⁻⁴⁵

In this article, a combination of coaxial electrospinning and carbonization at 1000 °C under nitrogen is used for the fabrication of SCNFs. In this way, the carbon shell can wrap tightly around the SiNP-CNT composite core, thereby minimizing the volume expansion of SiNPs. The conductive network formed by CNTs in the core can then act as pathways for electron transport between SiNP-SiNP or SiNP-carbon shell, as illustrated in **Figure 1**. After characterizing the morphology and coaxial structure of these SCNFs, they were applied as anodes in LIBs to investigate their electrochemical performance.

Experimental

Preparation of SiNP-CNT-core/carbon-shell nanofibers

The SCNFs used in this study were prepared by the coaxial electrospinning of a mixture of SiNPs, CNTs, and polyvinylpyrrolidone (PVP) in a co-solvent of acetone and *N,N*-dimethylformamide (DMF) (w:w = 1:1) for the core, and polyacrylonitrile (PAN) in DMF for the shell, as illustrated in **Figure S1** (Supplementary Information). Prior to use, the multi-walled CNTs were modified by a wet chemical oxidative process;⁴⁶⁻⁴⁸ in which carboxylic acid groups were attached to the CNT sidewalls, thereby increasing the accessibility of its surface to metal precursors in the aqueous solution. This, in turn, increased the deposition of metal and ensured a good dispersion in the polymer solution. After electrospinning, the SCNFs were thermally treated to stabilize and carbonize the PAN shell, as per a previously reported process.⁴⁹ For

comparative purposes, SiNP-core/carbon-shell coaxial-structured nanofibers (SNFs) were also prepared without CNTs.

Characterization of Morphology

The morphology of the SCNFs was investigated by scanning electron microscopy (SEM), using a MIRAIIXMH-Tescan (USA) with a Noble Target Sputter coating system; and by transmission electron microscopy (TEM) on a Tecnai G2 T-20S (FEI). The core-shell structure of the SCNFs was assessed using a water contact angle (WCA) method, which exploits the difference in the affinity for water between the hydrophobic PAN polymer shell and hydrophilic PVP polymer core. Thus, a high water contact angle on the electrospun SCNF membrane indicates a PVP core wrapped in a PAN shell, which is the desired core-shell structure of the SCNFs. Further confirmation of the SCNF structure was provided by high-resolution SEM and TEM images.

Thermogravimetric/differential thermal analyses (TG/DTA) of PAN, PVP, and the as-electrospun SCNF membrane were performed under both a nitrogen atmosphere and air using a SH IN2920 (TA Instruments, USA). Measurements were recorded over a temperature range of 25–700 °C, with a heating rate of 10 °C·min⁻¹. These analyses provided information regarding the remaining weight of PAN and PVP in the SCNFs after carbonization, as well as the relative weight of Si.

Preparation of LIBs and electrochemical characterization

SCNF-based anodes were electrochemically tested to investigate the effect of varying the CNT content of their core on LIB performance. For these tests, coin-type half cells were first prepared by employing lithium foil as both the reference and counter electrodes. The working

electrodes were prepared as follows: First, SCNFs with different amounts of CNTs in their core were mixed with Super P and polyvinylidene fluoride (PVDF, $M_w=180,000$, Sigma Aldrich Chemical, USA) to a ratio of SCNFs:Super P:PVDF = 70:15:15 by weight, to which was added 1-Methyl-2-pyrrolidinone (NMP, 99.5%, Sigma Aldrich Chemical, USA) to form a homogeneous slurry. This slurry was then pasted onto copper current collectors (18- μm thick Cu foil, Hohsen, Japan) to a thickness of 70–80 μm using the doctor blade method. The pasted electrodes were dried in a vacuum oven at 80 °C for 24 hours, and then punched to form circular discs. A SNF-based electrode (without CNTs) was prepared under the same conditions, and used as a control to assess the expansion of the SCNF electrodes.

The CR2032 coin cells were assembled in an Ar-filled glove box, with a 1M LiPF_6 solution in a mixture of ethylene carbonate (EC) and dimethyl carbonate (DMC) (1:1 = v:v, Soulbrain Co. Ltd., Korea) used as the electrolyte. A Hipore SV718 film (20- μm thickness, Asahi Kasei Chemicals Corporation, Japan) was used as the separator. These cells were then subjected to galvanostatic charge and discharge (same charge/discharge current) with an applied voltage cutoff of 0.05~2.0 V vs. Li/Li^+ using a TOSCAT-3100U battery tester (Toyo system Co. Ltd., Japan). The resulting electrochemical performance, as characterized and discussed in this article, was based on the mass of both Si and C in the anode materials.

Results and discussion

Core-shell structure and morphology of coaxially electrospun fibers

In order to validate the core-shell structure of the SNFs (without CNTs) and SCNFs (with 1 wt% of CNTs), the WCA of the SNF and SCNF fiber membranes was measured and found to

be close to that of PAN, as shown in **Figure S2** (Supplementary Information). This indicates that the SiNP-CNT/PVP composite of the core is wrapped by a PAN shell, confirming the fabrication of a core-shell structure in coaxially electrospun fibers.

The effect of varying the amount of CNTs on morphology of the coaxially electrospun SCNFs is demonstrated by the SEM images of as-electrospun coaxial fibers shown in **Figure 2**. From this, we can see those fibers containing up to 1 wt% of CNTs exhibit smooth and unique shapes, with no evidence of SiNPs or CNTs jutting out from the fiber surface; implying that a good core-shell structured fiber was achieved by coaxial electrospinning. In contrast, the as-electrospun fibers containing 2–10 wt% of CNTs in the core do show clusters of SiNPs on the fiber surface, the density of these clusters increasing with the amount of CNTs in the core. It is already known that CNTs are a good electrically conductive material, and under the applied high voltage of electrospinning can become highly charged and preferentially attracted to the collector faster than other components. This disrupts the stable state of the shell and core flows in the jet, the blockage of the shell by CNTs causing SiNPs to be drawn out of the core. However, the high spin rate of a CNT-containing electrospinning precursor causes SCNFs to have a smaller diameter than that of SNFs; and thus, coaxially electrospun fibers with moderate amounts of CNTs (<1 wt%) can form a core/shell structure. Nevertheless, with higher amounts of CNTs (2–10 wt%), this core/shell formation is inhibited. **Figure 3** shows high-magnification SEM images of core-shell structured SNFs and SCNFs with 1 wt% of CNTs, in which it can be seen that both have a 500-nm diameter and a SiNP core wrapped by a PAN shell.

The distribution of SiNPs in the core of the electrospun fibers was investigated before and after carbonization, with **Figures 4(a)** and **(b)** showing TEM images of the as-electrospun SNFs and SCNFs, respectively. In either instance, it is evident that a core of SiNPs with a particle size

of 50–100 nm is wrapped by a PAN shell. Conversely the TEM images of the carbonized SNFs and SCNFs shown in **Figure 4(c)** and **(d)**, respectively, show 200-nm diameter fibers with a 50-nm thick carbon shell layer. It is therefore evident that during carbonization the PVP in the core of these fibers is burn out, leaving SiNPs in the core of SNFs and a SiNP-CNT composite in the core of SCNFs. Meanwhile, the PAN shell is carbonized, transforming to carbon with a residual weight of around 60 %. This process is demonstrated by the TG thermograms provided in the Supplementary Information (**Figure S3**). In this, the mass component of SiNPs in carbonized SCNFs is determined over a temperature range 25–700 °C in air. The residual 50 wt% of solids is found to be mainly SiNPs, and not SiO₂, because the thermal oxidation of silicon is usually performed at a temperature of between 800 and 1200 °C.⁵⁰ With the mass ratio of SiNPs:carbon (SiNPs:C = 1:1) as a basis, the weight of SCNFs was used to analyze the electrochemical performance data.

The high-resolution TEM images of the SiNP-CNT composite shown in **Figure 4(f)** reveal that CNTs measuring approximately 20 nm in diameter and 10 μm in length completely fill the space between SiNPs in the core. This composite structure of CNTs and SiNPs should improve the electrical connectivity between SiNPs in the core matrix, which would in turn lead to a performance improvement in LIBs.

Electrochemical performance

Based on the mass ratio SiNPs:C (1:1), and the theoretical capacities of 4200 mAh/g for Si and 372 mAh/g for C, the theoretical capacity of SCNFs is 2286 mAh/g. Since the working electrodes consist of 70 wt% of SCNFs, 15 wt% of Super P, and 15 wt% of binder, a current of 1660 mA/g was applied as 1C for testing the electrochemical performance in the potential range

of 0.05–2.0 V vs. Li⁺/Li. All results discussed henceforth are therefore based on the weight of both Si and C. **Figure 5** shows the battery performance of SNF- and SCNF-based working electrodes with different amounts of CNTs, with their respective voltage profiles for the first cycles at a C/10 rate given in **Figure 5(a)**. We can see from this that the delithiation curve of SNF (without CNTs) exhibits an initial discharge capacity of 1230 mAh/g, and a corresponding coulombic efficiency (CE) of 76 %; whereas the curves for SCNFs with moderate amounts of CNTs show higher initial discharge capacities of 1400 mAh/g (CE = 79%) and 1500 mAh/g (CE = 87%) with CNT contents of 0.5 and 1 wt%, respectively. This supports the notion that the addition of CNTs into SCNFs can form a conductive network in the fiber core, which acts as a pathway for electron transport between SiNP–SiNP and SiNP–carbon shell. However, as the amount of CNTs in SCNFs is increased beyond 1 wt%, the initial discharge capacity is reduced, as shown in the inset of **Figure 5(a)**. This suggests that higher CNT loadings disrupts the core-shell structure of the fibers, resulting in initial discharge capacities of 1440, 1380, and 1290 mAh/g with CNT contents of 2, 5, and 10 wt%, respectively. It should be noted, however, that even these reduced values are still higher than that of SNFs. The decomposition of these fibers was further investigated through cycling tests, with **Figure 5(b)** showing the cycle performance of these electrodes at 1C. It is evident from this that after 100 cycles of charging and discharging, the core-shell structured electrodes with SNFs, and SCNFs with 0.5 and 1 wt% CNTs, exhibit discharge capacities of 450, 700 and 1000 mAh/g, respectively. Meanwhile, the discharge capacities of SCNFs with 2, 5, and 10 wt% of CNTs in the core are reduced to approximately 200 mAh/g as a result of their poor core-shell structure. This can be explained by the SEM observation of SiNPs and CNTs extending beyond the core of SCNFs, which would lead to SiNPs being directly exposed to the electrolyte. This poor structure also reduces the electrical

connectivity and resistance to Si expansion; and thus, although they may exhibit a high initial capacity, this becomes seriously decomposed after several charge/discharge cycles.

As shown in **Figure 5**, the highest SCNF performance is achieved with a CNT-SiNP composite (mass ratio 1:100) in the core. In the first cycle, this electrode exhibits an initial capacity of 1764 mAh/g for lithiation and 1500 mAh/g for delithiation, with a CE of 87 %. This is not only higher than the values of pure Si⁵ and Si composites,^{6,8-10} but is also close to that of coaxial-structured SiNPs/C fibers without CNTs obtained in previous studies,^{3,4} implying a stable SEI formation due to the coaxial structure of the electrodes. Furthermore, the initial discharge capacity based on Si alone is ~3295 mAh/g, which compared to the theoretical capacity of Si (~4200 mAh/g), shows that the contribution of SiNPs to the discharge capacity is 78.5 % higher than that reported by Hwang et al.³ In that study, SiNPs contributed ~70% to the discharge capacity, despite being based on a 3579 mAh/g theoretical capacity of Si. A decrease in the discharge capacity of Si was attributed to “dead” SiNPs, *i.e.*, those not electrically connected to the carbon shell.³ Thus, with an optimal amount of CNTs added to form a composite with SiNPs in the core, this electrical connection issue can clearly be improved.

Figure 6 shows the electrochemical performance of a SCNF working electrode with 1 wt% of CNTs. In this, the rate capabilities are shown at different C rates, increasing from C/10 to 10C and subsequently returning to C/10, as displayed in **Figure 6(a)** and **(b)**. In response to this, the capacity decreases from 1500 to 750 mAh/g, then increases back to 1505 mAh/g. Therefore, even though the applied current increases 100-fold, the capacity remains at just 50 % of its original value. The capacity retention at high rate is attributed to the enhanced electrical conductivity of the SCNF electrode, which is achieved by two separate means: Firstly, the 1D-structured carbon fibers of SCNFs can provide conductive pathways for electron diffusion³.

Secondly, the addition of CNTs to the core of SCNFs improves the connectivity between SiNPs. Thus, in the final cycle (C/10), even at a high C rate (10C) the capacity of the SCNFs is well maintained (1505 mAh/g), being as high as that (1500 mAh/g) in the first cycle at the same C/10 rate. This elastic capability is made possible by the stability of the SEI layers and robust structure of SCNFs. This advantage is also evident in the cycling performance of SCNFs at 1C rate for 100 cycles, as shown in **Figure 6(c)** and **(d)**. In this, it is clear the capacity is maintained at around 1000 mAh/g, or 74.1% of the original capacity (1350 mAh/g). Furthermore, the CE reaches 98 % by the 4th cycle, and is maintained at ~99 % at the 100th cycle. This enhancement of the CE and capacity retention over a large number of cycles is indicative that the electrochemical performance of SCNFs is significantly improved by incorporating a SiNP-CNT composite core wrapped in a carbon shell.

Assessment of SCNF anode material

Although the penetration of electrolyte into the core region causes a volume expansion in Si subjected to a large number of cycles,³ the structure of SCNFs can improve the electrochemical performance by reducing this volume change and forming a stable SEI. To investigate this further, a SCNF-anode was assessed by SEM and compared against SiNP- and SNF-anodes. **Figure 7** shows the volume change in each of these electrodes before and after 100 cycles. In **Figure 7(a)** and **(b)**, we see that the thickness of a SiNP-only electrode increases from 80 μm to 200 μm , representing an expansion of 250 vol%. In contrast, the expansion of SNFs (**Figure 7(c,d)**) and SCNFs (**Figure 7(e,f)**) are 125 and 121 vol%, respectively. This indicates that the core-shell structure of SNFs and SCNFs significantly reduces the volume expansion of Si. **Figure 7(g)** and **(h)** provide a higher magnification SEM view of the cycled SCNFs in 7(f), from which it can be seen that the core-shell structure of the single SCNF fiber in 7(h) is

maintained after cycling. The irregularly-shaped particles observed on the fiber surface are identified as binder and Super-P, both of which were added in the preparation of the LIB devices.

In order to confirm the formation of stable SEI, EIS measurements are carried out for both SNF- and SCNF-based LIB devices before and after cycling for 100 cycles in the frequency range 10^6 – 5^{-1} Hz, as shown in **Figure 8**. The Nyquist plots of both devices with SNFs and SCNFs after cycling show similar diameters comparing to their original plots before cycling. It indicates that the interfacial resistances of SNFs and SCNFs are constant throughout cycling, leading to stable SEI formation, as well as they have core/shell structure. The carbon shell restricts boundary and prevents the SEI layers in the core and on SiNP surfaces.³ The semicircles of SNFs and SCNFs in the intermediate frequency range are attributed to impedance related to the charge transfer process at the SEI. The value of charge resistance of SCNFs, determined from the Z' of the intermediate frequency side semicircle in the Nyquist plots, is $\sim 65 \Omega$, smaller than that of SNFs ($\sim 100 \Omega$). It indicates that the addition of CNTs in the core of SCNFs improves the electronic conductivity in the core, leading to restriction of negative effects of SEI layers in the core.

Conclusions

Electrospun SiNP-CNT-core carbon-shell structured nanofibers (SCNFs), used as the anode of a LIB, were successfully fabricated by coaxial electrospinning and subsequent carbonization at 1000 °C for 1 h in nitrogen. This process was confirmed to produce a carbon shell encapsulating a SiNP-CNT composite core, though SEM and TEM analysis showed that this was dependent on the amount of CNTs in the core. Specifically, those SCNFs containing

less than 1 wt% of CNTs retain a core-shell structure, whereas higher loadings (>1 wt%) cause the this structure to be broken. Analysis of the cycling performance of SCNF-based anodes showed that SCNFs with 1 wt% of CNTs have a high initial capacity of 1500 mAh/g in the first cycle at 0.1C, and retained 50 % of their capacity when cycled at 10C. They were also shown to retain a capacity of 74.1 %, and a CE of 99 %, over the course of 100 cycles at 1C. These results indicate that a core-shell structure can significantly reduce the volume change of Si, and addition of CNTs in the core can improve the electrical conductivity of the anode. As such, SCNF-based electrodes show great promise for use in LIBs.

Acknowledgements

This work was financially supported by grants from the Fundamental R&D Program for Core Technology of Materials by the Ministry of Knowledge Economy and the Government-Funded General Research & Development Program by the Ministry of Trade, Industry and Energy, Republic of Korea.

Notes and references

^a Department of Chemical Engineering and Center for Chemical Technology, Hankyong National University, Gyeonggi-do, Anseong-si 456-749, Korea.

^b Division of Advanced Materials, Korea Research Institute of Chemical Technology, Jang-dong 100, Daejeon, Yuseong 305-600, Korea.

* Corresponding author 1: Tel: +82-31 670 5202 Fax: +82-31 675 9604

E-mail: jspark@hknu.ac.kr

** Corresponding author 2: Tel: +82-42-860-7207

E-mail: ykang@kRICT.re.kr

† Electronic Supplementary Information (ESI) available: Experimental details, Water contact angle measurements, TGA data, EDS data, and TEM images.

1. K. T. Lee and J. Cho, *Nano Today*, 2011, **6**, 28-41.
2. H. Wu and Y. Cui, *Nano Today*, 2012, **7**, 414-429.
3. T. H. Hwang, Y. M. Lee, B.-S. Kong, J.-S. Seo and J. W. Choi, *Nano Lett.*, 2012, **12**, 802-807.
4. B.-S. Lee, S.-B. Son, K.-M. Park, J.-H. Seo, S.-H. Lee, I.-S. Choi, K.-H. Oh and W.-R. Yu, *J. Power Sources*, 2012, **206**, 267-273.
5. L. Ji and X. Zhang, *Carbon*, 2009, **47**, 3219-3226.
6. S.-M. Jang, J. Miyawaki, M. Tsuji, I. Mochida and S.-H. Yoon, *Carbon*, 2009, **47**, 3383-3391.

7. G. K. Simon, B. Maruyama, M. F. Durstock, D. J. Burton and T. Goswami, *J. Power Sources*, 2011, **196**, 10254-10257.
8. L. Ji and X. Zhang, *Electrochem. Commun.*, 2009, **11**, 1146-1149.
9. L. Wang, C. X. Ding, L. C. Zhang, H. W. Xu, D. W. Zhang, T. Cheng and C. H. Chen, *J. Power Sources*, 2010, **195**, 5052-5056.
10. Q. Si, K. Hanai, T. Ichikawa, A. Hirano, N. Imanishi, Y. Takeda and O. Yamamoto, *J. Power Sources*, 2010, **195**, 1720-1725.
11. K. Fu, L. Xue, O. Yildiz, S. Li, H. Lee, Y. Li, G. Xu, L. Zhou, P. D. Bradford and X. Zhang, *Nano Energy*, 2013, **2**, 976-986.
12. J. Y. Howe, D. J. Burton, Y. Qi, H. M. Meyer Iii, M. Nazri, G. A. Nazri, A. C. Palmer and P. D. Lake, *J. Power Sources*, 2013, **221**, 455-461.
13. L. Xue, K. Fu, Y. Li, G. Xu, Y. Lu, S. Zhang, O. Toprakci and X. Zhang, *Nano Energy*, 2013, **2**, 361-367.
14. J. W. Choi, J. McDonough, S. Jeong, J. S. Yoo, C. K. Chan and Y. Cui, *Nano Letters*, 2010, **10**, 1409-1413.
15. N. Liu, L. Hu, M. T. McDowell, A. Jackson and Y. Cui, *ACS Nano*, 2011, **5**, 6487-6493.
16. K. Kang, H.-S. Lee, D.-W. Han, G.-S. Kim, D. Lee, G. Lee, Y.-M. Kang and M.-H. Jo, *Appl. Phys. Lett.*, 2010, **96**, -.
17. C. K. Chan, R. N. Patel, M. J. O'Connell, B. A. Korgel and Y. Cui, *ACS Nano*, 2010, **4**, 1443-1450.
18. S.-H. Baek, J.-S. Park, E.-J. Bae, Y.-I. Jeong, B.-Y. Noh and J. H. Kim, *J. Power Sources*, 2013, **244**, 515-520.

19. X. Zhao, X. Rui, W. Zhou, L. Tan, Q. Yan, Z. Lu and H. H. Hng, *J. Power Sources*, 2014, **250**, 160-165.
20. M. Battaglia, S. Piazza, C. Sunseri and R. Inguanta, *Electrochem. Commun.*, 2013, **34**, 134-137.
21. J. Ha and U. Paik, *J. Power Sources*, 2013, **244**, 463-468.
22. L. Yue, W. Zhang, J. Yang and L. Zhang, *Electrochim. Acta*, 2014, **125**, 206-217.
23. Y. Hwa, W.-S. Kim, B.-C. Yu, J.-H. Kim, S.-H. Hong and H.-J. Sohn, *J. Power Sources*, 2014, **252**, 144-149.
24. R. C. de Guzman, J. Yang, M. M.-C. Cheng, S. O. Salley and K. Y. Simon Ng, *J. Power Sources*, 2014, **246**, 335-345.
25. Y.-S. Ye, X.-L. Xie, J. Rick, F.-C. Chang and B.-J. Hwang, *J. Power Sources*, 2014, **247**, 991-998.
26. D. Y. Kim, J. Suk, D. W. Kim, Y. Kang, S. H. Im, Y. Yang and O. O. Park, *J. Mater. Chem. A*, 2014.
27. J. Suk, D. Y. Kim, D. W. Kim and Y. Kang, *J. Mater. Chem. A*, 2014, **2**, 2478-2481.
28. L. Zou, L. Gan, R. Lv, M. Wang, Z.-h. Huang, F. Kang and W. Shen, *Carbon*, 2011, **49**, 89-95.
29. M.-H. Park, M. G. Kim, J. Joo, K. Kim, J. Kim, S. Ahn, Y. Cui and J. Cho, *Nano Lett.*, 2009, **9**, 3844-3847.
30. T. Song, J. Xia, J.-H. Lee, D. H. Lee, M.-S. Kwon, J.-M. Choi, J. Wu, S. K. Doo, H. Chang, W. I. Park, D. S. Zang, H. Kim, Y. Huang, K.-C. Hwang, J. A. Rogers and U. Paik, *Nano Lett.*, 2010, **10**, 1710-1716.

31. T. Song, H. Cheng, H. Choi, J.-H. Lee, H. Han, D. H. Lee, D. S. Yoo, M.-S. Kwon, J.-M. Choi, S. G. Doo, H. Chang, J. Xiao, Y. Huang, W. I. Park, Y.-C. Chung, H. Kim, J. A. Rogers and U. Paik, *ACS Nano*, 2011, **6**, 303-309.
32. H. Ma, F. Cheng, J. Y. Chen, J. Z. Zhao, C. S. Li, Z. L. Tao and J. Liang, *Advanced Materials*, 2007, **19**, 4067-4070.
33. Y. Yao, M. T. McDowell, I. Ryu, H. Wu, N. Liu, L. Hu, W. D. Nix and Y. Cui, *Nano Lett.*, 2011, **11**, 2949-2954.
34. Z. Dong, S. J. Kennedy and Y. Wu, *J. Power Sources*, 2011, **196**, 4886-4904.
35. N. T. Hieu, J. Park and B. Tae, *Mater. Sci. Eng., B*, 2012, **177**, 205-209.
36. J. Guo, A. Sun and C. Wang, *Electrochem. Commun.*, 2010, **12**, 981-984.
37. H. S. Choi, J. G. Lee, H. Y. Lee, S. W. Kim and C. R. Park, *Electrochim. Acta*, 2010, **56**, 790-796.
38. Q. Si, K. Hanai, T. Ichikawa, A. Hirano, N. Imanishi, O. Yamamoto and Y. Takeda, *J. Power Sources*, 2011, **196**, 6982-6986.
39. Y. Liu, K. Huang, Y. Fan, Q. Zhang, F. Sun, T. Gao, Z. Wang and J. Zhong, *Electrochim. Acta*, 2013, **102**, 246-251.
40. L. Qiao, X. Sun, Z. Yang, X. Wang, Q. Wang and D. He, *Carbon*, 2013, **54**, 29-35.
41. J. Bae, *J. Solid State Chem.*, 2011, **184**, 1749-1755.
42. Y. Zhang, X. G. Zhang, H. L. Zhang, Z. G. Zhao, F. Li, C. Liu and H. M. Cheng, *Electrochim. Acta*, 2006, **51**, 4994-5000.
43. J. Shu, H. Li, R. Yang, Y. Shi and X. Huang, *Electrochem. Commun.*, 2006, **8**, 51-54.
44. K.-S. Park, K.-M. Min, S.-D. Seo, G.-H. Lee, H.-W. Shim and D.-W. Kim, *Mater. Res. Bull.*, 2013, **48**, 1732-1736.

45. M. Zhang, X. Hou, J. Wang, M. Li, S. Hu, Z. Shao and X. Liu, *J. Alloys Compd.*, 2014, **588**, 206-211.
46. Y.-C. Chiang, W.-H. Lin and Y.-C. Chang, *Appl. Surf. Sci.*, 2011, **257**, 2401-2410.
47. T. A. Saleh, *Appl. Surf. Sci.*, 2011, **257**, 7746-7751.
48. A. de Moraes, L. M. D. Loiola, J. E. Benedetti, A. S. Gonçalves, C. A. O. Avellaneda, J. H. Clerici, M. A. Cotta and A. F. Nogueira, *J. Photochem. Photobiol., A*, 2013, **251**, 78-84.
49. S. K. Nataraj, K. S. Yang and T. M. Aminabhavi, *Prog. Polym. Sci.*, 2012, **37**, 487-513.
50. A. G. Aberle, S. Glunz and W. Warta, *J. Appl. Phys. (Melville, NY, U. S.)*, 1992, **71**, 4422-4431.

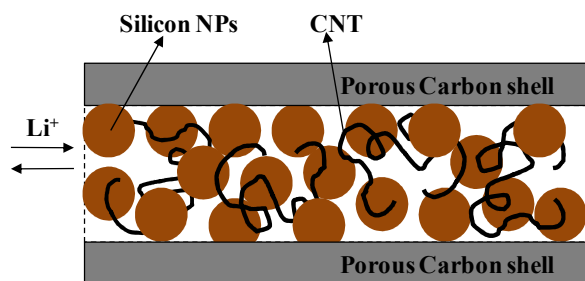


Figure 1: Schematic depicting the structure and operation of a SCNF.

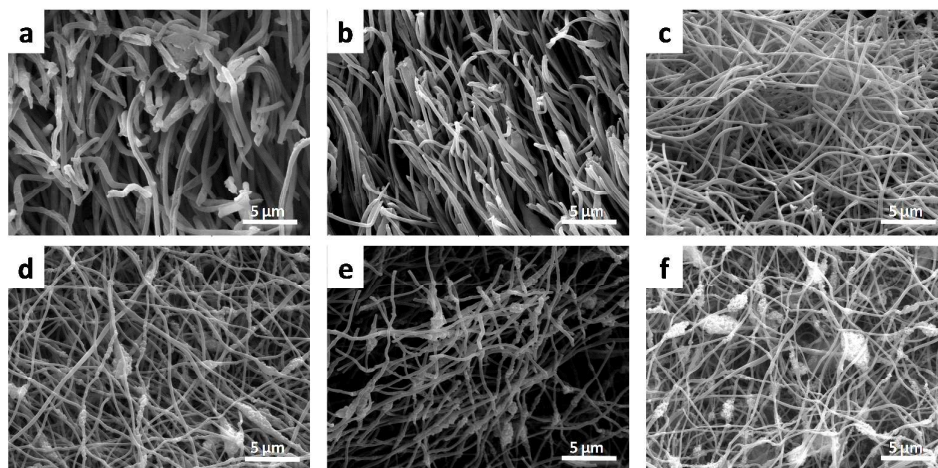


Figure 2: SEM images of (a) as-electrospun SiNP-core/carbon-shell nanofibers (SNFs) and SiNP-CNT-core/carbon-shell nanofibers (SCNFs) with different CNT:SiNP ratios of (b) 0.5, (c) 1, (d) 2, (e) 5, and (f) 10 wt%.

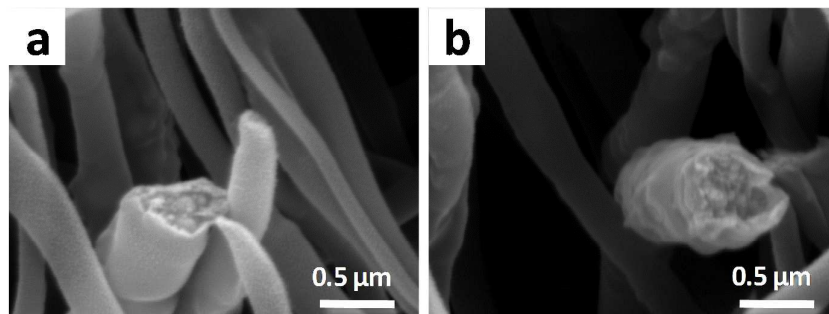


Figure 3: SEM images of (a) as-electrospun SiNP-core/carbon-shell nanofibers (SNFs) and (b) as-electrospun SiNP-CNT-core/carbon-shell nanofibers (SCNFs) with 1 wt% of CNTs.

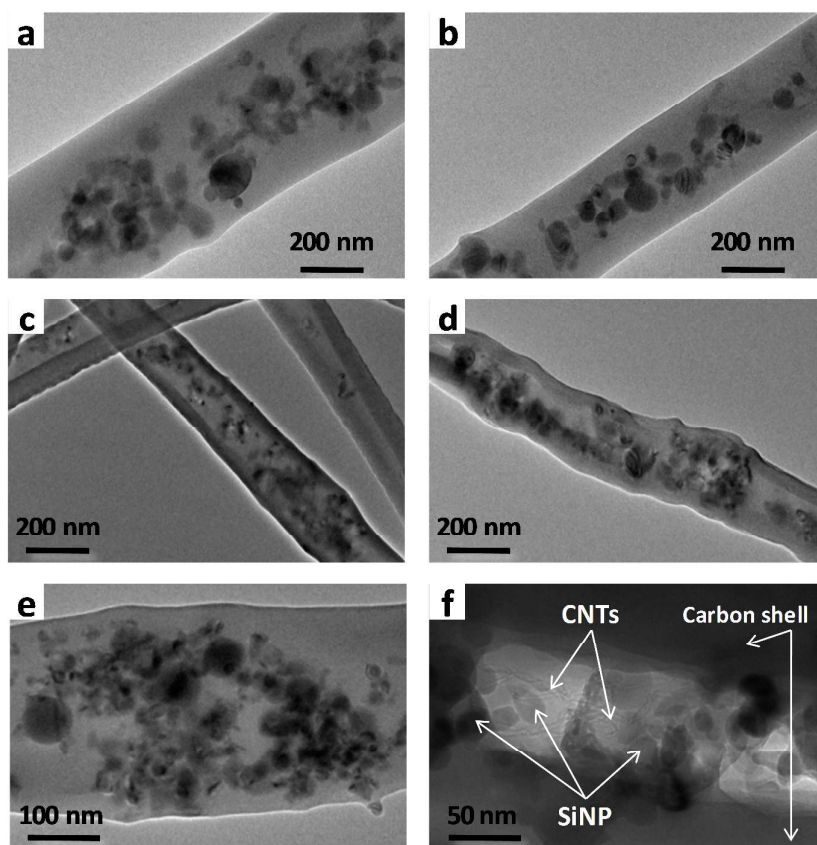


Figure 4: TEM images of (a) as-electrospun SiNP-core/carbon-shell nanofiber (SNF); (b) as-electrospun SiNP-CNT-core/carbon-shell nanofiber with 1 wt% of CNTs (SCNF); (c,e) carbonized SNFs; and (d,f) SCNFs carbonized in nitrogen at 1000 °C for 1 h.

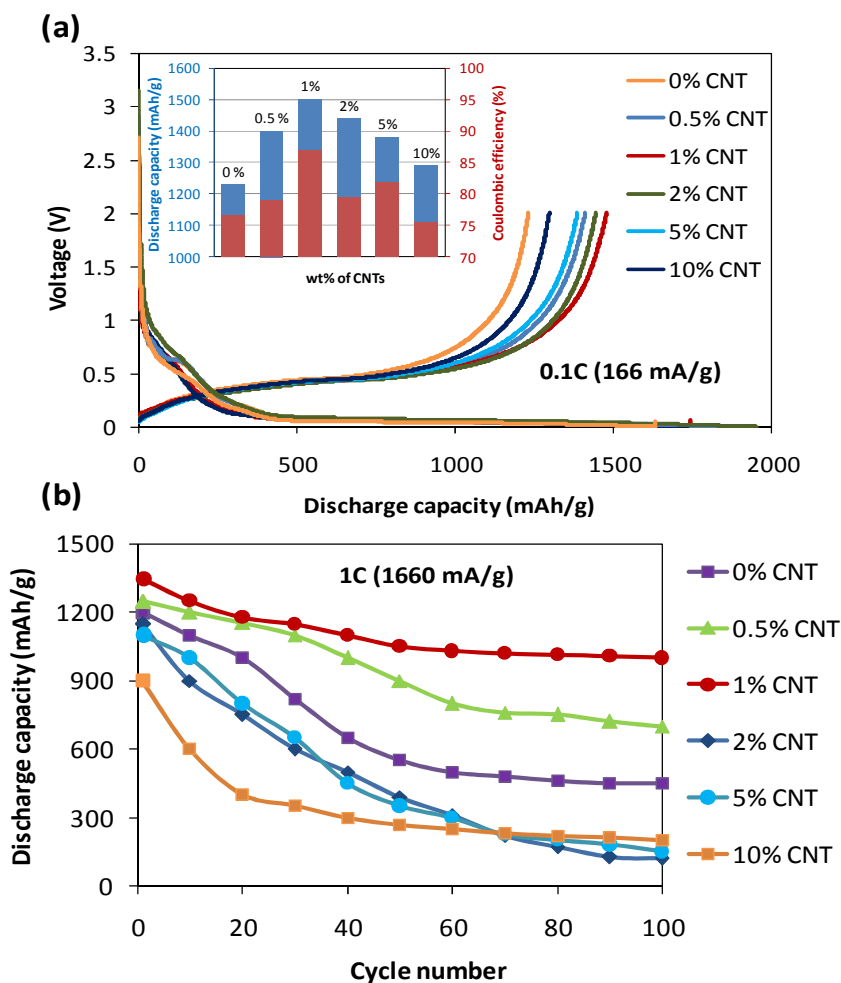


Figure 5: Electrochemical performance of SCNF-based working electrodes. (a) Voltage profiles of the first cycle for SNF (no CNTs) and SCNF with different amounts of CNTs (CNTs:SiNPs = 0.5, 1, 2, 5, 10 wt%) at C/10 (0.166 A/g). The inset in (a) shows: (blue diagram) initial discharge capacity and (red diagram) coulombic efficiency for each electrode. (b) Cycle performance at 1C (1.66 A/g).

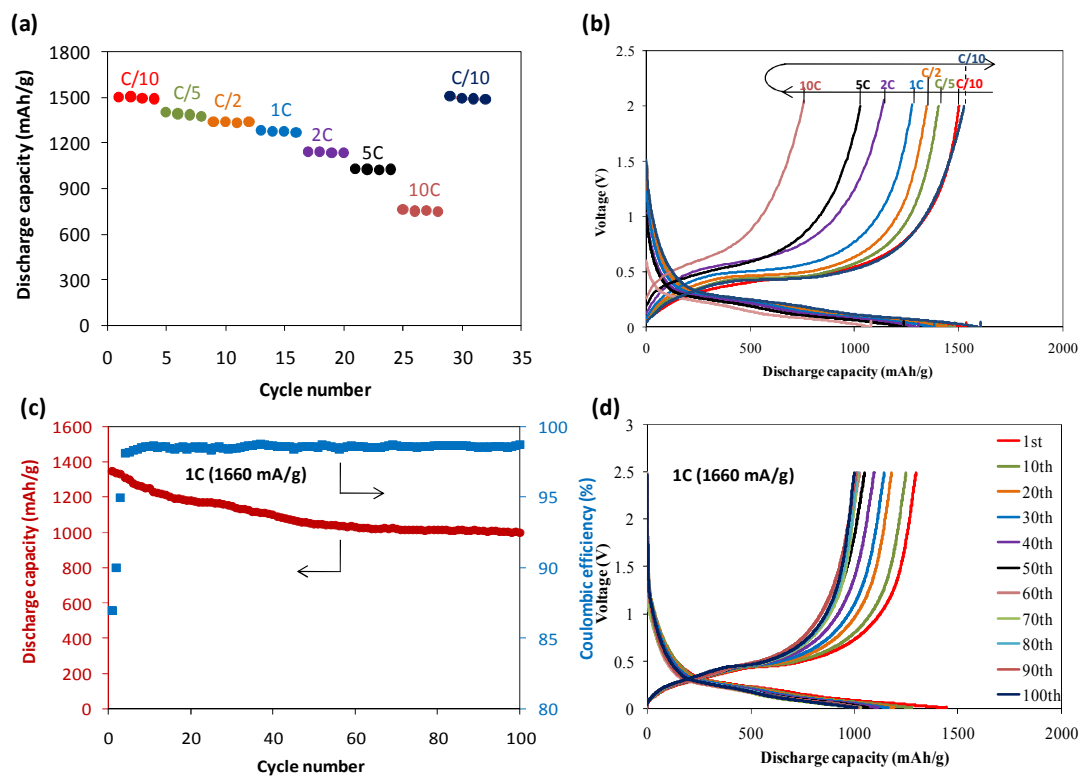


Figure 6: Electrochemical performance of a SCNF working electrode with 1 wt% of CNTs. (a) C-rate test and (b) respective voltage profiles. (c) Cycling performance, including capacity and coulombic efficiency, at 1C (1.66 A/g) rate. (d) Voltage profiles of SCNFs in (c).

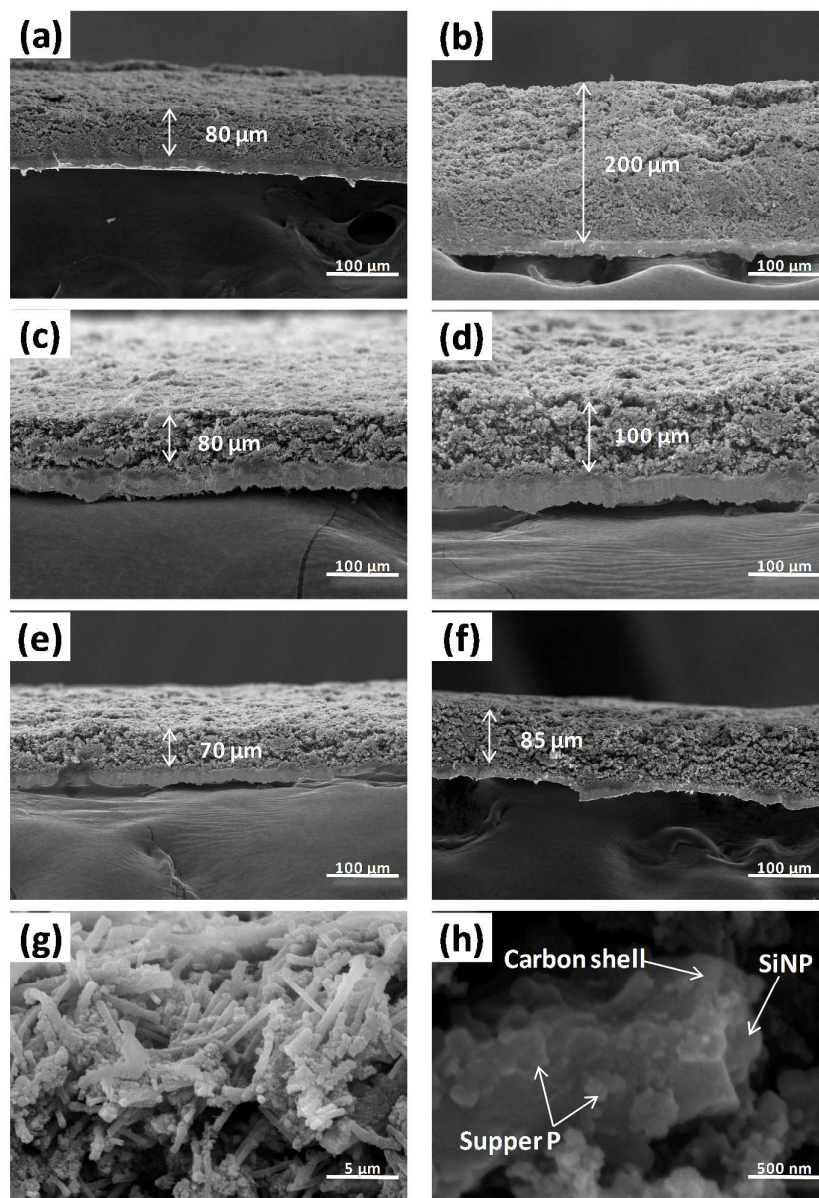


Figure 7: Cross-sectional SEM images of working electrodes based on: (a,b) SiNPs only; (c,d) SiNP-core/carbon-shell nanofibers (SNFs); (e,f) SiNP-CNT-core/carbon-shell nanofibers with 1 wt% of CNTs (SCNFs). Images were taken either (a,c,e) before or (b,d,f) after performance testing for 100 cycles, with (g) and (h) being high resolution SEM images of (f).

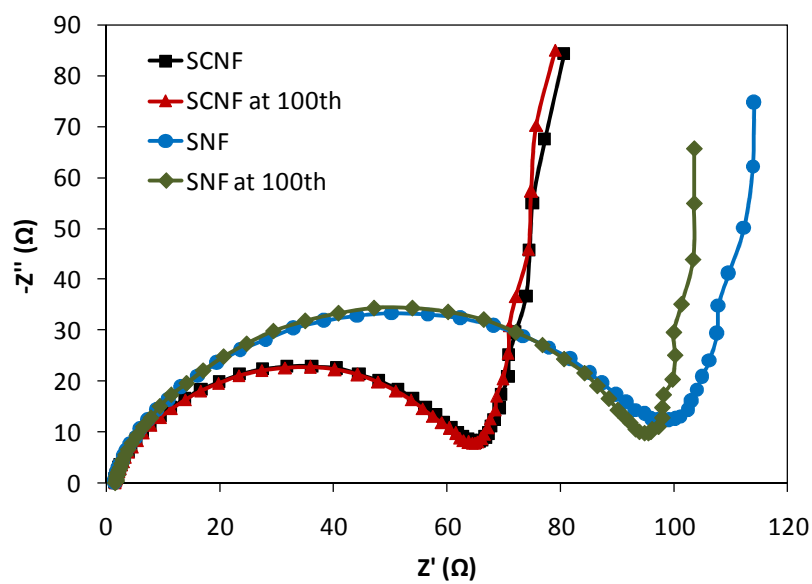
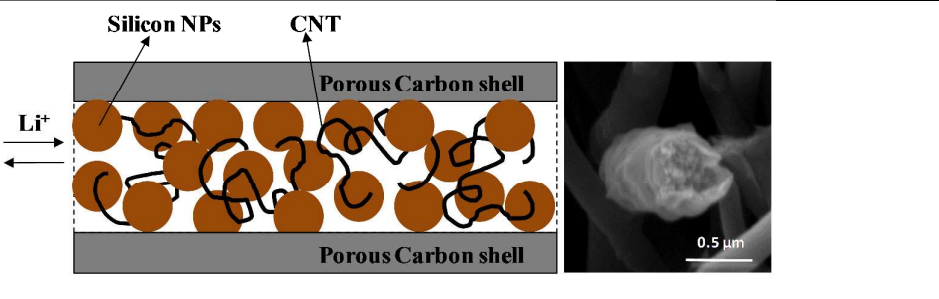


Figure 8: Nyquist plots of the SNF- and SCNF-based anodes before and after cycling performance test for 100 cycles in the frequency range 10^6-5^{-1} Hz.

Contents entry

Colour graphic:	 <p>The figure consists of two parts. On the left is a schematic diagram of a core-shell structure. It shows a central orange circle representing a Silicon NP (Silicon Nanoparticle). This is surrounded by a network of black wavy lines representing CNTs (Carbon Nanotubes). The entire structure is enclosed within a grey rectangular frame labeled 'Porous Carbon shell'. To the left of the shell, there are two horizontal arrows pointing in opposite directions, labeled 'Li+', indicating the movement of lithium ions. On the right is a grayscale SEM (Scanning Electron Microscope) image of a single particle, showing a porous, irregular shell structure. A scale bar at the bottom right of the SEM image is labeled '0.5 μm'.</p>
Text:	Core-shell Si-CNT@C as anode in LIBs can minimize volume change and improve conductivity, enhancing the battery performance.